archives
of thermodynamics
Vol. **40**(2019), No. 1, 127–143
DOI: 10.24425/ather.2019.128294

Heat transfer and pressure drop characteristics of the silicone-based plate heat exchanger

TOMASZ MUSZYŃSKI[*a]
RAFAŁ ANDRZEJCZYK[a]
IL WONG PARK[b]
CARLOS ALBERTO DORAO[b]

[a] Gdansk University of Technology, Faculty of Mechanical Engineering, Narutowicza 11/12, 80-233 Gdańsk, Poland

[b] Norwegian University of Science and Technology, Høgskoleringen 1, 7491 Trondheim, Norway

Abstract The paper presents an experimental investigation of a silicone based heat exchanger, with passive heat transfer intensification by means of surface enhancement. The main objective of this paper was to experimentally investigate the performance of a heat exchanger module with the enhanced surface. Heat transfer in the test section has been examined and described with precise measurements of thermal and flow conditions. Reported tests were conducted under steady-state conditions for single-phase liquid cooling. Proposed surface modification increases heat flux by over 60%. Gathered data presented, along with analytical solutions and numerical simulation allow the rational design of heat transfer devices.

Keywords: Heat transfer coefficient; Heat exchangers; Enhanced surface; Wilson's plot method

Nomenclature

A	–	surface of heat transfer, m^2
c_p	–	specific heat, J/kg K
D	–	jet orifice diameter, m
F	–	flow orientation correction factor

*Corresponding Author. Email: tommuszy@pg.gda.pl

h	–	channel height, m
k	–	total heat transfer, W/m^{2}K
LMTD	–	logarithmic mean temperature difference, K
$\dot{m}$	–	mass flow of fluid, kg/s
Nu	–	Nusselt number
P	–	pressure, Pa
Pr	–	Prandtl number
ΔP	–	pressure drop, Pa
Re	–	Reynolds number
S_D	–	jet orifice surface, m^2
T	–	temperature, K
v	–	velocity, m/s
$\dot{V}$	–	volumetric flow rate, m^3/s
q	–	heat flux, W/m^2
$\dot{Q}$	–	heat flow, W

Greek symbols

α	–	heat transfer coefficient, W/m^{2}K
δ	–	thickness of membrane, m
ρ	–	density, kg/m^3
λ	–	thermal conductivity, W/mK
μ	–	dynamic viscosity, Pa s
ν	–	kinematic viscosity, m^2/s

Superscripts

c	–	cold
h	–	hot

1 Introduction

Nowadays, increasing efficiency of energy utilization became a universal trend both in industry and households. It's driven both by the rising cost of energy resources and environmental considerations. Significant gains can be made also in these areas by increasing the efficiency of energy utilization, i.e., recovering low-grade waste heat [1], or improving process efficiency [2]. Boiling and condensation are associated with large rates of heat transfer because of the latent heat of evaporation and because of the enhancement of the level of turbulence between the liquid and the solid surface [3,4]. Achieving of high heat fluxes can be obtained by means of numerous technologies: microchannels [5], microjets [6], hybrid microjet-microchannels [7], etc. The high convection of jet impingement commonly prolongs the heat flux range where partial boiling is available [8].

The passive enhanced techniques include: artificial surface roughness, including protrusions, sand grains, and knurling; displaced promoters, such

as flow disturbers located away from the heat transfer surface; vortex generators, like twisted tape insert, coiled wires inserts, threads, internally coiled tubes. It is a well-known fact that any enhancement technique will introduce additional fluid pressure drop, and often the ratio of pressure drop increase is larger than that of heat transfer enhancement [9,10]. Hence it is very important on how to quantitatively evaluate the thermohydraulic performance improvement for a given enhancement technique. Performance evaluation is normally made by comparing the performance of the enhanced surface with a corresponding referenced structure [11].

The heat exchanger effectiveness is defined by the ratio of the actual enthalpy change of working medium to the maximum enthalpy difference attainable under ideal working conditions. The efficiency of heat exchangers is often taken as a decisive parameter in process design [12]. The detailed project and optimization should take account of the problem requirements, such as durability, operating temperature, volume of the heat exchanger, required material, cost, and so on, which possess a major impact on the selection of technical solution and project profitability ahead of design [13]. The industrial processes require a new generation of heat exchangers which have better performance and exclude all shortcomings of the currently used constructions while maintaining low investment cost [14]. Highly compact and highly efficient heat exchanger constructions are investigated to develop highly efficient systems [15,16].

The modeling and models validation for heat exchangers used in the various process is an important task towards optimal system design. Models, currently used in the literature, are capable of predicting the working parameters, and system response [17,18]. Cost-effectiveness and increasing efficiency lead research towards new technologies of heat transfer enhancement in heat exchangers design. One of the methods is to reduce the plant investment cost by replacing conventional metallic heat exchangers with plastic components, due to its lower mass and cost [19]. Unfortunately, optimization and design improvement of heat exchangers are very challenging tasks. Experimental studies aimed at optimizing their geometries tend to be costly and time-consuming because of a considerable number of geometrical parameters [20,21].

As mentioned earlier, enhancement of the heat transfer and its prediction is an essential step in the design of a variety of devices in the power and process engineering. This study focuses on obtaining experimental values of heat transfer in the silicone-based heat exchanger. The primary objectives

of the present study are to:

- provide an experimental database for single-phase forced convection on the enhanced surface,
- recognize the effect surface enhancement on heat transfer and pressure drop,
- provide an experimental database on the silicone-based heat exchanger,
- provide a guide for selecting a suitable surface enhancement for specific fluid flow regime.

2 Test facility

The present study shows results of steady-state heat transfer experiments, conducted for single phase cooling in order to obtain working fluids temperatures and heat fluxes. It consisted of the heat exchanger, fluid supplying system, the measuring devices, constant temperature bath, and chiller. The cold working fluid was fed by a pulsation-free gear pump from a supply tank. The desired fluid flow rate was obtained by means of the power inverter and flow control valve. Detailed view of heat exchanger module is presented in next section.

The temperature was measured at the inlets and outlets of the heat exchanger by T-type thermocouples. All thermocouples are pre-calibrated with a dry box temperature calibrator. They are connected to the National Instruments data acquisition set. The signal from thermocouples was processed with the aid of the LabVIEW application [22]. Heat is supplied by a constant temperature bath in a hot water circuit. Total power input is determined by measuring the volumetric flow rate and temperature rise. During tests, the heat exchanger was capable of dissipating up to 232 W. The entire setup was thermally insulated.

The heat source is a laboratory grade ultra-thermostat with electric heater power of 2000 W, with temperature stability of $\pm 0.05\,^{\circ}\mathrm{C}$. Ultra-thermostat can operate with different working fluids, i.e distilled water, water solutions of glycols and silicone oils. Thus it is possible to obtain a wide range of parameter change and study the influence of fluid properties on the present system. Cold water circulates in a second circuit with heat rejection controlled by an industrial grade chiller.

The feed pump is a magnetic gear pump – Verder VS120. The use of magnetic drive means that the device fully impermeable. It allows the

pump to operate at a high pressure, high temperatures, with chemically reactive media, such as glycols, saline, fluorinated agents, etc.

The flow rate is measured using a Coriolis mass flow meter, the advantage of this type of measurement is a simultaneous measure of the mass and density of the pumped liquid. Heat is supplied to them by the water circulating in a constant temperature bath. The total power of the heat exchanger is determined by the mass and energy balance. Measurements take place in steady-state conditions, in order to exclude the heat capacity of the casing of the system. The amount of heat transferred is determined at each measurement point.

Pressure drop measurement is carried out at the cold water circuit using the piezoelectric smart differential pressure transmitter. Microprocessor control enables temperature and hysteresis compensation, also it allows to provide an extended linear temporal stability. The measuring range of the transmitter is from 5 kPa to 500 kPa, and the measuring accuracy is 0.065% FS (full scale). The pressure at the inlet and outlet of the heat exchanger is also measured using conventional pressure transducers. At the inlet, an absolute pressure transducer with a measuring range of 0 to 400 kPa is mounted. At the outlet gauge pressure transducer with the range of 0–600 kPa is installed. This along with measured barometric pressure allows for the exact determination of the parameters of the fluid in the measuring point and doubling the measured pressure drop. It is important to verify the operation of the system and capture any hardware failure. On the side of the hot fluid, the temperature at the inlet and outlet of the heat exchanger, is measured by means of thermocouples T in class 1. Also a control gauge pressure transmitters in the range 0 to 2500 kPa and accuracy of 0.3% FS are installed at the inlet and outlet.

As part of the thermal and flow measurement the following parameters are recorded: the hot fluid temperature at the inlet (T_h') and outlet (T_h'') of the exchanger, the temperature of the cold fluid at the inlet (T_c') and outlet (T_c'') of the exchanger, and volumetric flow rate of the two fluids, and also the pressure at the inlet and the outlet of the heat exchanger.

In order to determine the reliability of the experimental results, an uncertainty analysis was conducted on all measured quantities as well as the quantities calculated from the measurement results. Uncertainties were estimated according to the standard procedures described by the National Institute of Standards and Technology (NIST) [23]. Overall, the uncertainty in the calculated Nusselt number is lower than 29%. Uncertainties

of the other calculated variables are shown in Tab. 1.

Table 1: Experimental parameters.

Parameter	Value	Unit
Medium	water	–
Flow rate	0.016–0.006	kg/s
Pressure	120	kPa
Surface area	4×10^{-4}	m^2
Temp. cold in	280.6	K
Temp. hot in	313.1	K
Channel height	4×10^{-3}	m
Plate thickness:		
Aluminium	1×10^{-3}	m
Silicone	0.515×10^{-4}	m
Thermal conductivity:		
Aluminium	207	W/mK
Silicone	149	W/mK

3 Heat exchanger design

The research object is a micro heat exchanger, a recuperator type, see Fig. 1. Its essential core is a series of plates. Various geometries are created by introducing plates and spacers with different thickness. These plates are made of polytetrafluoroetylene (PTFE). Heat exchange between the working fluids is performed through plate made of the aluminum alloy EN AW-1050A, with a heat exchange surface of 4×10^{-4} m, or 5.50×10^{-4} m thick polished silica plate. Because the compression of spacers and membranes may cause some distortion in the collector (made with PMA) to prevent leakage between the channels of the collector seal with high-temperature silicone compound was applied. Same types of plates with enhancement surface are shown in Figs. 2 and 3.

In Fig. 2, a SEM photo is shown from etched silicon under directional conditions. The random nanostructures are made by a DRIE using the black silicon method [24,25]. These surfaces were manufactured on

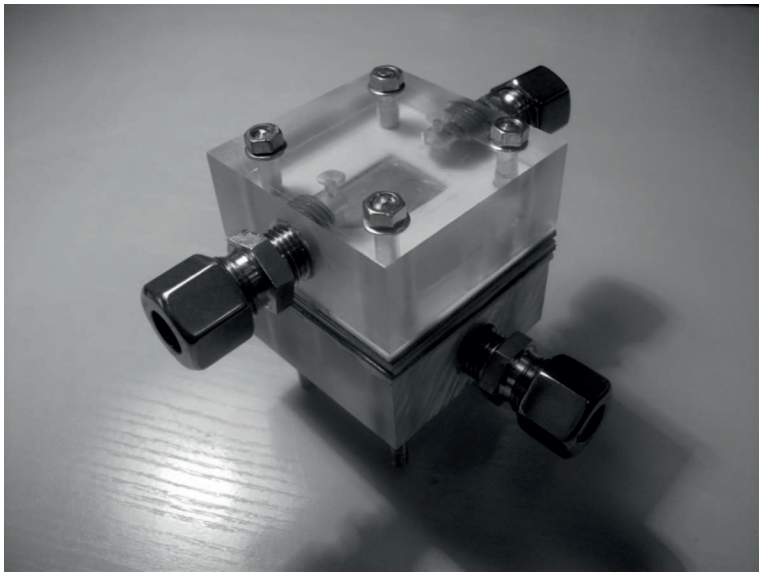

Figure 1: View of the tested heat exchanger.

silicon wafers using a combination of random nanostructuring processes, microlithography, and thin hydrophobic polymer coating. The spikes are 5×10^{-6} m in height and a few microns in width. The origin of micromasks is caused by native oxide, dust and so on which is present on the wafer before etching. But, it is also formed during the etching because silicon oxide particles coming from the plasma are adsorbing at the silicon surface or because of the oxidation of the surface together with the angle-dependent ion etching of this oxide layer. Another source of particles during etching which will act as micromasks is the redepositioning of mask material due to imparting ions. The root mean square of the standard height deviation of a surface scan on a polished wafer is typically less than 1×10^{-9} m.

Gathered was data for four heat exchanger plates during experiments, i.e., polished aluminum, knurled aluminum, polished silica, and ion charged plasma silica, fastened in the heat exchanger module. Figure 4 presents heat exchangers hydraulic characteristics for selected geometries of cold water flow. As expected, the pressure drop for various enhancement techniques was indistinguishable in selected flow range.

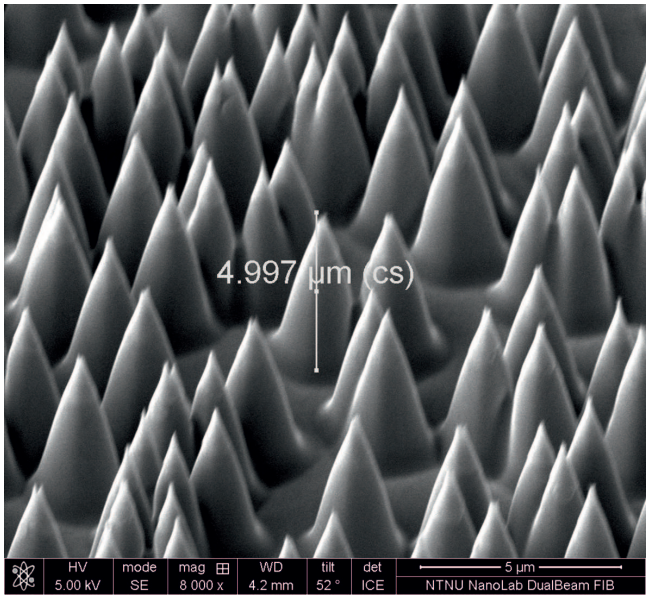

Figure 2: Scanning electron microscope (SEM) image of the silica plate with enhancement.

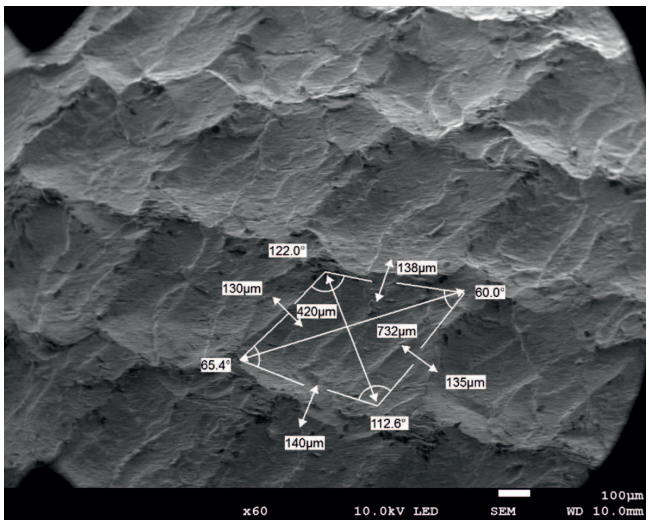

Figure 3: SEM image of the aluminum plate with enhancement.

4 Experimental data reduction

Wilsons plot method is a graphical way of calculating heat transfer coefficient of given working fluid, based on the total heat transfer in the heat exchanger for varying fluid flow rate [17].

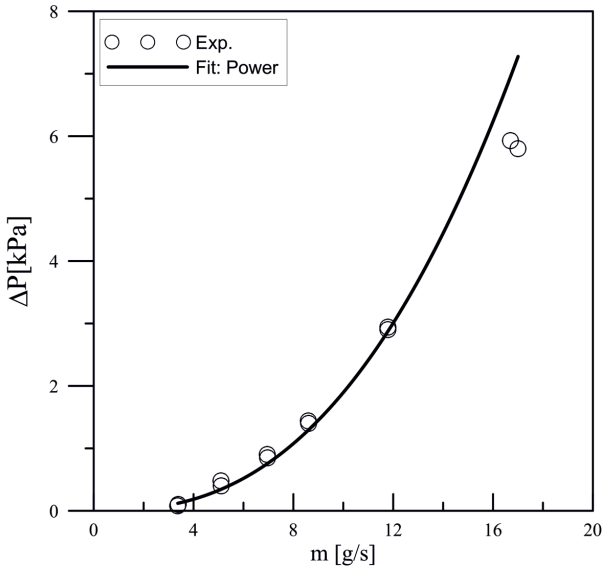

Figure 4: Hydraulic characteristics of the tested heat exchanger.

During thermal measurements, hydraulic characteristics of test heat exchanger were gathered. Obtained results are presented in Fig. 4. Further analysis is focused on the flow range from 0.006 to 0.016 kg/s what corresponds to Reynolds number from 500 to 1200. As can be seen pressure drop is not linear in that region, therefore turbulent flow is expected, mainly due to inlet effects at the manifold.

Fluid overflows the heat exchangers membrane from both sides. Thus the heat exchange surface is, in fact, the wetted surface of membrane, i.e., 4×10^{-4} m^2. Flow arrangement has a co-current pattern. If we also assume a constant heat flux on the heat exchange surface, thus logarithmic mean temperature difference can be used as an acting temperature gradient between two fluids. It can be written as

$$\mathrm{LMTD} = \frac{(T'_h - T'_c) - (T''_h - T''_c)}{\ln\left(\dfrac{T'_h - T'_c}{T''_h - T''_c}\right)}. \tag{1}$$

The heat flux can be written as

$$q = F\,k\,\mathrm{LMTD}\,. \tag{2}$$

The correction parameter (F) is calculated based on the obtained temperature differences in crossflow heat exchangers. Due to the low flow rate variations during the experiment, the correction factor value was always close to 1, and it was assumed as constant in further calculations. Then the total amount of heat transferred is

$$\dot{Q} = q\,A\,. \tag{3}$$

Based on calculated heat flux, the total heat transfer coefficient is calculated from Eq. (5). For further calculations, heat absorbed by cold medium was taken into account. The heat exchanger was capable of exchanging up to 100 W of thermal energy at LMTD of 30 K, corresponding to 245 W/m^2 heat flux.

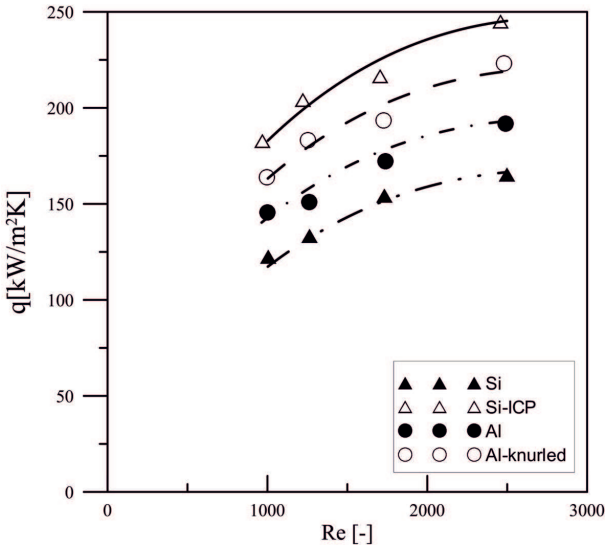

Figure 5: Experimentally obtained heat flux in the heat exchanger for LMTD of 30 K, with various heat transfer membranes in function of hot fluid Reynolds number.

Direct comparison of experimentally obtained heat flux density with various materials and surfaces is presented in Fig. 5. Non-modified reference was used to evaluate the effect of the enhanced surface on heat transfer.

During tests, constant temperature difference at inlets was kept. Due to the variations on the outlet of the heat exchanger, LMTD was in the range from 31.6 to 30 K. As can be seen the plane silicone plate yields lowest results due to its perfectly flat surface. Reference aluminum plate was well grinded, which will result in surface roughness two orders of magnitude higher than the reference silicone plate.

Surprisingly, the black silicone – ICP treated silicone introduces only 5 μm surface roughness, but due to the large increase of surface area, transferred heat was over 50% higher than in the plane silicone plate, and over 20% higher than the plane aluminum plate. Knurling applied on the aluminum plate increases its surface by approx. 10% with the selected pattern, therefore the difference between both aluminum plates can be attributed only to the increased surface area.

In order to calculate the heat transfer coefficient we can assume identical surface area on both sides of the heat exchanging surface therefore total heat transfer coefficient can be expressed as

$$\frac{1}{k} = \frac{1}{\alpha_c} + \frac{1}{\frac{\lambda}{\delta}} + \frac{1}{\alpha_h}\,. \tag{4}$$

Nusselt number correlations are usually formed based on the well-known Dittus-Boelter correlation

$$\mathrm{Nu} = C_0\,\mathrm{Re}^n\,\mathrm{Pr}^m\,, \tag{5}$$

where C_0, n, and m are experimental factors whereas Nusselt, Reynolds, and Prandtl numbers are described as

$$Nu = \frac{\alpha D}{\lambda}\,, \qquad \mathrm{Re} = \frac{\rho \dot{V} D}{\mu S_D}\,, \qquad \mathrm{Pr} = \frac{\mu c_p}{\lambda}\,.$$

After rearranging Eq. (8) heat transfer coefficient takes the form

$$\alpha = C_0 \left(\frac{\rho \dot{V} d}{\mu S_D}\right)^n \left(\frac{\mu c_p}{\lambda}\right)^m \left(\frac{\lambda}{D}\right)\,. \tag{6}$$

For specified flow geometry and constant fluid properties in the specified temperature range, Eq. (9) simplifies to

$$\alpha = C_1 \dot{V}^n, \tag{7}$$

where C_1 is a constant and $\dot{V}$ is fluids volumetric flow rate. Thus, the heat transfer coefficient of a cold fluid, while sustaining constant flow parameters on the hot fluid side, can be written as

$$\frac{1}{k} = \frac{a}{\dot{V}_c^n} + b\,, \tag{8}$$

where $a = {}^{1}\!/_{C_c}$ and $b = \frac{1}{\frac{\lambda}{\delta}} + \frac{1}{\alpha_h}$. Therefore the heat transfer coefficient is a linear function of volumetric flow rate of the cold fluid, where coefficient a is functions gradient and fb is an ordinate as depicted in Fig. 6.

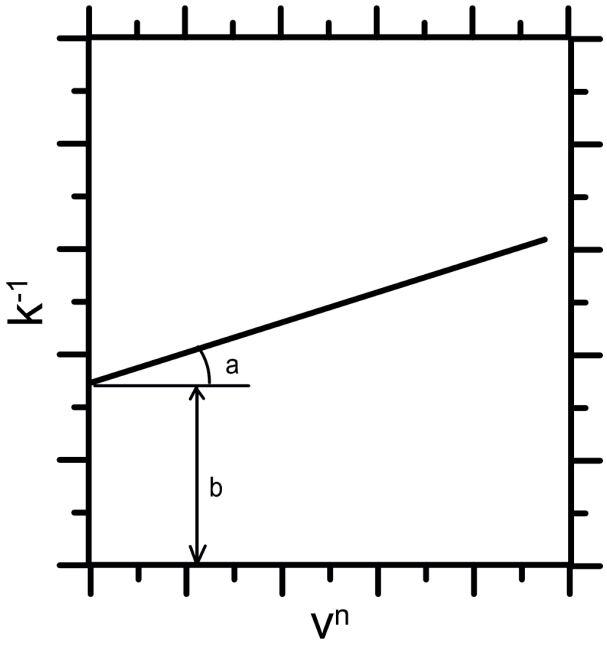

Figure 6: Graphical scheme for calculating heat transfer coefficient by Wilsons plot method.

Based on experimental data and given data reduction procedure it is possible to calculate the heat transfer coefficient on the hot fluid side. Due to the low Reynolds numbers and inlet manifold geometry, it can be assumed that the flow is in the mixed-turbulent regime. The n parameter to which the flow rate is raised usually ranges from 0.6 to 0.7, but best results are obtained if the experimental fit of this coefficient is carried out. In presented cases, this coefficient was selected as 0.7. The value of ordinate is

calculated by extrapolation of experimental data to the vertical axis, which corresponds to infinite heat transfer coefficient of the cold fluid. With the negligible low thermal resistance of a membrane, the ordinate is a heat transfer coefficient of the hot fluid. The scheme for calculating the heat transfer coefficient is presented in Fig. 6, which presents the linear regression values for experimental series grouped in constant cold fluid velocities. The intersection of the linear extrapolation of experimental data yields the heat transfer coefficient on the hot fluid side. The resulting heat transfer coefficient of hot fluid from experimental data was calculated by Eq. (7). The heat transfer coefficient calculations by Wilson's method were conducted for the experimental parameters grouped in Tab. 1. The main error of approximation comes from the root mean square error of linearization depicted in Fig. 6, which for the experimental conditions yields 99.96% to 97.26%. Therefore assumed discrepancy associated with the measurement error is assumed to be below 30%.

The doubled height of the channel ($2h$) was taken as a characteristic dimension in calculating the Nusselt and Reynolds number.

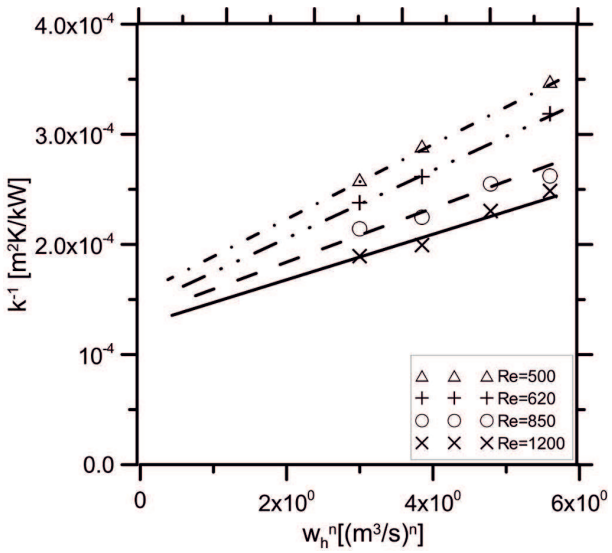

Figure 7: Graphical scheme for calculating heat transfer coefficient, for the case of cold fluid jet Re = 1200.

Figures 8 and 9 present experimental data series with experimental Nusselt number values, calculated with Wilsons plot method, for constant cold fluid velocity, and 7 °C supply temperature. Experimental data were collected

for hot water was a heat supply for constant temperature level of 40 °C.

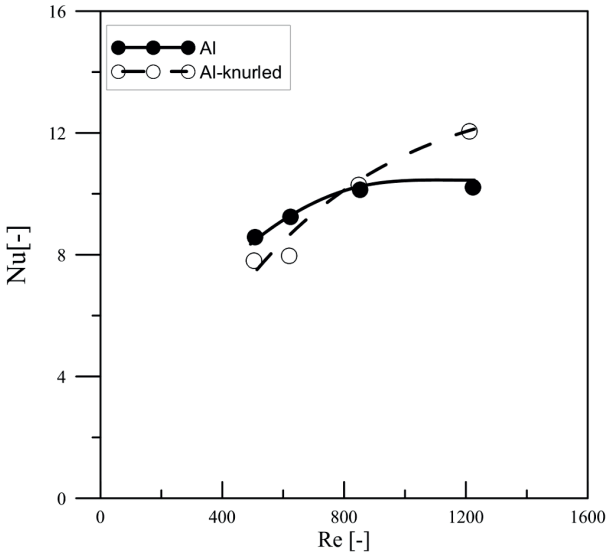

Figure 8: Comparison of Nusselt number values obtained in case of plain and enhanced aluminum plate in function of cold fluid Reynolds number.

As can be seen for low Reynolds numbers, obtained Nusselt numbers for enhanced and reference plates are similar, within the error of the method. The advantage of the enhanced surface is more pronounced on the higher flow rate. Therefore suggesting that heat transfer coefficient is also influenced by included surface modification. And the increased amount of transferred heat is attributed not only to the larger surface area. As can be seen the surface enhancement during the ion charged plasma technique provides an enhancement in the whole tested flow range. Alternatively, knurling provides measurable effects only in higher fluid flow rates. It is possible that the dimples created by knurling are blocking the flow in near wall region for low fluid velocities and only in higher flow rates, where it acts as a turbulence promoter, flow turbulence level is increased by a separation and reattachment mechanism. Due to the Wilsons plot error obtained heat transfer coefficient values depend on the experimental data fit, as explained earlier.

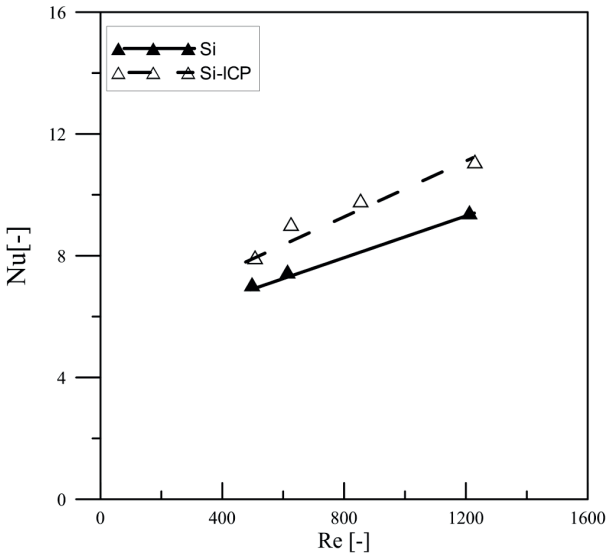

Figure 9: Comparison of Nusselt number values obtained in case of plain and enhanced silicone plate in function of cold fluid Reynolds number.

5 Conclusions

As the first step of this work, an experimental study was undertaken in order to obtain accurate pressure drop values during the water flow in heat exchanger module. The range of experimental conditions covered were: four mass velocities and four different surfaces. The existing experimental facility allowed to run tests under the experimental campaign acquired over 200 experimental points.

The study revealed that proper selection of the heat exchanger material and passive enhancement technique is of primary importance. Selection of ion charged plasma technique for passive heat transfer enhancement can increase the heat transfer rate up to 50%, with unnoticeable effect on pressure drop.

Acknowledgments The work was partially funded by the Research Council of Norway under the FRINATEK Project 231529.

Received 23 December, 2017

References

[1] Muszynski T.: *Design and experimental investigations of a cylindrical microjet heat exchanger for waste heat recovery systems*. Appl. Therm. Eng. **115**(2017), 782–792. DOI:10.1016/j.applthermaleng.2017.01.021.

[2] Kowalczyk C., Rolf R.M., Kowalczyk B., Badyda K.: *Mathematical model of combined geat and power plant using GateCycle TM software*. J. Power Technol. **95**(2015), 183–191.

[3] Mikielewicz D., Jakubowska B.: *Prediction of flow boiling heat transfer coefficient for carbon dioxide in minichannels and conventional channels*. Arch. Thermodyn. **37**(2016), 2, 89–106. DOI:10.1515/aoter-2016-0014.

[4] Mikielewicz D., Jakubowska B.: *Calculation method for flow boiling and flow condensation of R134a and R1234yf in conventional and small diameter channels*. Polish Marit. Res. **24**(2017), 141–148. DOI:10.1515/pomr-2017-0032.

[5] Cho E.S., Choi J.W., Yoon J.S., Kim M.S.: *Experimental study on microchannel heat sinks considering mass flow distribution with non-uniform heat flux conditions*. Int. J. Heat Mass Tran. **53**(2010), 9, 2159–2168. DOI:10.1016/j.ijheatmasstransfer.2009.12.026.

[6] Muszynski T., Mikielewicz D.: *Structural optimization of microjet array cooling system*. Appl. Therm. Eng. **123** (2017), 103–110. DOI:10.1016/j.applthermaleng.2017.05.082.

[7] Muszynski T., Andrzejczyk R.: *Heat transfer characteristics of hybrid microjet – microchannel cooling module*. Appl. Therm. Eng. **93**(2016), 1360–1366. DOI:10.1016/j.applthermaleng.2015.08.085.

[8] Muszynski T., Mikielewicz D.: *Comparison of heat transfer characteristics in surface cooling with boiling microjets of water, ethanol and HFE7100*. Appl. Therm. Eng. **93**(2016), 1403–1409. DOI:10.1016/j.applthermaleng.2015.08.107.

[9] Muszynski T., Andrzejczyk R., Dorao C.A.: *Detailed experimental investigations on frictional pressure drop of R134a during flow boiling in 5 mm diameter channel: The influence of acceleration pressure drop component*. Int. J. Refrig. **82**(2017). DOI:10.1016/j.ijrefrig.2017.05.029.

[10] Muszynski T., Andrzejczyk R., Dorao C.A.: *Investigations on mixture preparation for two phase adiabatic pressure drop of R134a flowing in 5 mm diameter channel*. Arch. Thermodyn. **38**(2017), 3, 101–118. DOI:10.1515/aoter-2017-0018.

[11] Motyliński K., Kupecki J.: *Modeling the dynamic operation of a small fin plate heat exchanger- parametric analysis*. Arch. Thermodyn. **36**(2015), 3, 85–103. DOI:10.1515/aoter-2015-0023.

[12] Taler D., Ocłoń P.: *Thermal contact resistance in plate fin-and-tube heat exchangers, determined by experimental data and CFD simulations*. Int. J. Therm. Sci. **84**(2014), 309–322. DOI:10.1016/j.ijthermalsci.2014.06.001.

[13] Zhu Y., Hu Z., Zhou Y., Jiang L., Yu L.: *Discussion of the internal heat exchanger's effect on the organic rankine cycle*. Appl. Therm. Eng. **75**(2015), 334–343. DOI:10.1016/j.applthermaleng.2014.10.037.

[14] Wang Q., Zeng M., Ma T., Du X., Yang J.: *Recent development and application of several high-efficiency surface heat exchangers for energy conversion and utilization*. Appl. Energy. **135**(2014), 748–777.

[15] Bustamante J.G., Rattner A.S., Garimella S.: *Achieving near-water-cooled power plant performance with air-cooled condensers*. Appl. Therm. Eng. **105**(2016), 362–371. DOI:10.1016/j.applthermaleng.2015.05.065.

[16] Kupecki J., Badyda K.: *Mathematical model of a plate fin heat exchanger operating under solid oxide fuel cell working conditions*. Arch. Thermodyn. **34**(2013), 4, 3–21. DOI:10.2478/aoter-2013-0026.

[17] Muszynski T., Andrzejczyk R.: *Applicability of arrays of microjet heat transfer correlations to design compact heat exchangers*. Appl. Therm. Eng. **100**(2016), 105–113. DOI:10.1016/j.applthermaleng.2016.01.120

[18] Fratczak M., Nowak P., Czeczot J., Metzger M.: *Simplified dynamical input–output modeling of plate heat exchangers – case study*. Appl. Therm. Eng. **98**(2016), 880–893. DOI:10.1016/j.applthermaleng.2016.01.004.

[19] Trojanowski R., Butcher T., Worek M., Wei G.: *Polymer heat exchanger design for condensing boiler applications*. Appl. Therm. Eng. **103**(2016), 150–158. DOI:10.1016/j.applthermaleng.2016.03.004.

[20] Muszynski T., Koziel S.M.: *Parametric study of fluid flow and heat transfer over louvered fins of air heat pump evaporator*. Arch. Thermodyn. **37**(2016), 3, 45–62. DOI:10.1515/aoter-2016-0019.

[21] Andrzejczyk R., Muszynski T.: *Performance analyses of helical coil heat exchangers. The effect of external coil surface modification on heat exchanger effectiveness*. Arch. Thermodyn. **37**(2016) 4, 137–159. DOI:10.1515/aoter-2016-0032.

[22] National Instruments Coorporation LabVIEW User Manual. Ni.com (2013).

[23] Taylor B.N., Kuyatt C.E.: *Guidelines for evaluating and expressing the uncertainty of NIST measurement results*. NIST Tech. Note. **1297**(1994), 20. DOI:10.6028/NIST.TN.1900.

[24] Jansen H., de Boer M., Legtenberg R., Elwenspoek M.: *The black silicon method: a universal method for determining the parameter setting of a fluorine-based reactive ion etcher in deep silicon trench etching with profile control*. J. Micromech. Microeng. **5**(1995), 5, 115. DOI:10.1088/0960-1317/5/2/015.

[25] Park I.W., Fernandino M., Dorao C.A.: *Wetting state transitions over hierarchical conical microstructures*. Adv. Mater. Interfaces. 5(2018) 1701039. DOI:10.1002/admi.201701039.